ELSEVIER

Journal of Alloys and Compounds 323–324 (2001) 649–653

Journal of ALLOYS AND COMPOUNDS

www.elsevier.com/locate/jallcom

New excitement with crystal-field excitations

Albert Furrer*, Thierry Strässle, Daniel Rubio Temprano

Laboratory for Neutron Scattering, ETH Zurich and Paul Scherrer Institute, CH-5232 Villigen PSI, Switzerland

Abstract

The crystal field is one of the major interactions in rare-earth compounds. Neutron spectroscopy has become the key tool to measure the crystal-field transitions in metallic systems. This has been demonstrated for almost 1000 metallic rare-earth compounds in the past 30 years which resulted in a detailed understanding of the various physical effects caused by the crystal-field splitting. One may conclude that the determination and description of crystal fields in metallic rare-earth systems is now well established and has become a standard technique. Yet the past years have seen exciting developments in different applications where the crystal-field concept attained increasing and sometimes even crucial importance. This is exemplified for two applications: Firstly, the novel principle for cooling by adiabatic pressure application which is based on the occurrence of a pressure-induced structural and/or magnetic phase transition where the point symmetry at the rare-earth site is changed involving a change in the degeneracy of the crystal-field states. Secondly, the observation of anomalies in the linewidth of crystal-field transitions in high-temperature superconductors which reveals direct information on the doping and isotope dependence of the pseudogap.

Keywords: High-T_c superconductors; Intermetallics; Crystal and ligand fields; Heat capacity

1. Introduction

The crystal-field interaction in rare-earth compounds is responsible for an enormous variety of magnetic phenomena. The crystal field is based on the electrostatic potential at the rare-earth ion position which is defined by

$$V_{\mathrm{CF}}(\vec{r}) = \sum_i \frac{\rho(\vec{R}_i)}{|\vec{r} - \vec{R}_i|} \tag{1}$$

where $\rho(\vec{R}_i)$ denotes the charge distribution at the site $\vec{R}_i$ of the ith ligand ion. When considering only the ground-state J-multiplet of the rare-earth ion, the crystal-field Hamiltonian is most commonly expressed by

$$\hat{H}_{\mathrm{CF}} = \sum_{m,n} B_n^m \hat{O}_n^m \tag{2}$$

where B_n^m and $\hat{O}_n^m$ are, respectively, crystal-field parameters and Stevens operator equivalents [1]. Eq. (2) gives rise to a decomposition of the $(2J+1)$-fold degenerate ground-state multiplet into a series of crystal-field states Γ_i with energies E_i. The wave functions of the irreducible representations Γ_i are given by

$$|\Gamma_i\rangle = \sum_{M=-J}^{J} a_i(M)|M\rangle \tag{3}$$

All the thermodynamic magnetic properties such as the magnetization, the magnetic susceptibility, the Schottky heat capacity and the entropy are completely determined by the eigenvalues E_i and the eigenfunctions $|\Gamma_i\rangle$ of the crystal-field Hamiltonian (Eq. (2)).

By far the most unique and perhaps direct experimental method for the determination of the crystal-field interaction in metallic rare-earth compounds is provided by inelastic neutron scattering. This can immediately be seen from the thermal neutron cross section for the crystal-field transition $|\Gamma_i\rangle \rightarrow |\Gamma_j\rangle$ which in the dipole approximation is given by [2]

$$\frac{\mathrm{d}^2\sigma}{\mathrm{d}\omega \mathrm{d}\Omega} \propto F^2(Q) p_i |\langle \Gamma_j | \hat{J}_\perp | \Gamma_i \rangle|^2 \delta(E_i - E_j \pm \hbar\omega) \tag{4}$$

with

$$p_i = \frac{1}{Z} \exp\left\{ -\frac{E_i}{k_B T} \right\}$$

where $F(Q)$ is the magnetic form factor, Z the partition function, and $\hat{J}_\perp$ the component of the total angular momentum operator perpendicular to the scattering vector $\vec{Q}$. The crystal fields of roughly 1000 metallic rare-earth compounds have been investigated by neutron spectros-

*Corresponding author. Tel.: +41-56-310-2088; fax: +41-56-310-2939.

0925-8388/01/$ – see front matter
PII: S0925-8388(01)01025-8

copy up to the present time as summarised by Moze [3]. One may therefore conclude that the determination and the description of crystal fields in metallic rare-earth compounds is now well established and has become a standard technique. Yet the past years have seen exciting developments in different applications where the crystal-field concept attained increasing and sometimes even crucial importance. Two of these applications will be introduced and discussed in the following sections.

2. The barocaloric effect in $Pr_{1-x}La_xNiO_3$ and $Ce_{1-x}(La,Y)_xSb$

Upon the removal of a magnetic field from a material, the resulting reduction in magnetic spin alignment represents an increase in the material's spin entropy. If the field reduction is performed adiabatically, there will be a decrease in the temperature of the material which is called the magnetocaloric effect. Cooling rates of typically 1 K per 1 T field change have been achieved so far, with a maximum of about 4 K predicted for $Gd_5(Si_xGe_{1-x})$ which is called the 'giant' magnetocaloric effect [4]. Recently, a novel principle for cooling by adiabatic pressure application was introduced [5]. The principle of the barocaloric effect is based on the occurrence of a pressure-induced structural phase transition where the point symmetry at the rare-earth site is changed involving a change of the degeneracy of the crystal-field ground state. This is exemplified below for the rare-earth nickelates $Pr_{1-x}La_xNiO_3$.

Neutron diffraction and spectroscopy as well as magnetic susceptibility and heat capacity measurements were employed to characterize the physical properties of the compounds $Pr_{1-x}La_xNiO_3$ which undergo a structural phase transition (SPT) from a high-temperature $R\bar{3}c$ rhombohedral to a low-temperature orthorhombic *Pbnm* phase in the concentration range $0<x<0.7$ [6,7]. The temperature T_{SPT} is strongly dependent on the La concentration x: For $x=0$, we have $T_{SPT}\approx 700$ K, and $dT_{SPT}/dx\approx -1000$ K. The application of hydrostatic pressure was found to shift T_{SPT} typically by $dT_{SPT}/dp\approx -50$ K/GPa. The crystal-field ground state is a singlet in the *Pbnm* phase, whereas a non-Kramers doublet is the lowest crystal-field state in the $R\bar{3}c$ phase [7]. This has important consequences on the magnetic entropy which is defined by

$$S = -R\sum_i p_i \cdot \ell n p_i \qquad (5)$$

Fig. 1 shows that the entropies calculated from Eq. (5) for the two symmetries *Pbnm* and $R\bar{3}c$ differ by $\Delta S\approx 5.5$ J/mol·K over a wide temperature range, which enables cooling as indicated by the adiabatic pressure step $a\rightarrow b$.

We have studied the barocaloric effect for polycrystalline $Pr_{1-x}La_xNiO_3$ with $x=0.34$ [8] and more recently for $x=0.5$ and 0.6 [6]. For $x=0.34$ we found a tiny cooling

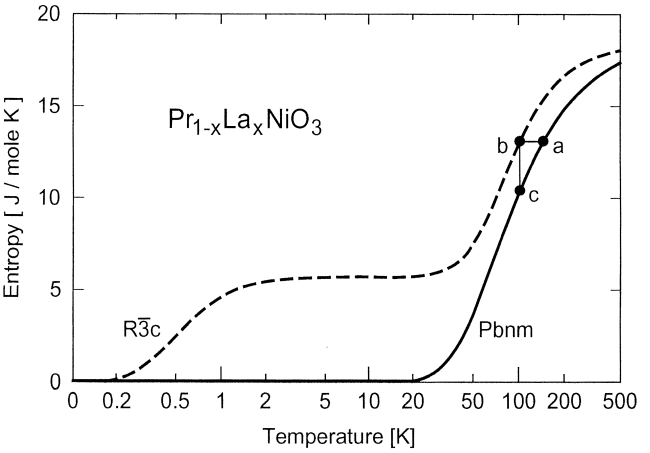

Fig. 1. Entropy calculated for the rhombohedral $R\bar{3}c$ and orthorhombic *Pbmn* phases of $Pr_{1-x}La_xNiO_3$. The entropy of the $R\bar{3}c$ phase vanishes at low temperatures due to the exchange interaction between the Pr^{3+} ions which was assumed to be of the order of 1 K.

effect of 0.1 K per 0.5 GPa pressure change at a working temperature around 350 K, but practically no cooling for $x=0.5$ and $x=0.6$ at working temperatures around 180 and 50 K, respectively. This is due to the fact that the expected cooling was largely compensated by the competing effects of pressure-induced elastic heating and friction, the latter being a particular problem in experiments on polycrystalline samples. We therefore conclude that efficient cooling can only be achieved by using ceramic or single-crystalline material. Moreover, efficient cooling is restricted to low temperatures, since the entropy of the phonons dominates the crystal-field entropy at temperatures above say 30 K. This was verified for CeSb as described in the following paragraphs.

The rare-earth compound CeSb orders antiferromagnetically below $T_N\approx 16$ K in various phases with characteristic ordering wave vectors $\vec{q}_o=(2\pi/a)\times(0,\ 0,\ q_o)$ with $1/2\leq q_o\leq 2/3$ [9,10]. The onset of magnetic ordering is accompanied by a structural phase transition from cubic to tetragonal symmetry [11]. The tetragonal state can also be realized by the application of uniaxial pressure along the [001] axis. As a result the magnetically ordered state can be reached for temperatures $T>T_N$, with $dT_N/dp\approx 8$ K/GPa [12] as visualized in the p–T phase diagram of Fig. 2.

The Ce^{3+} ions in CeSb experience the crystal-field interaction which splits the lowest J-multiplet of the Ce^{3+} ions into a ground-state doublet and an excited quartet at about 3 meV [13]. The cubic-to-tetragonal phase transition induced by uniaxial pressure splits the quartet into two doublets which lowers the entropy of the system. Furthermore, the entropy decrease is enhanced by the onset of magnetic ordering below T_N due to a complete lifting of the degeneracy of the crystal-field states through the Zeeman effect, thereby amplifying the barocaloric effect substantially. Fig. 2 shows the evolution of the entropy as a function of temperature and pressure. The key element is

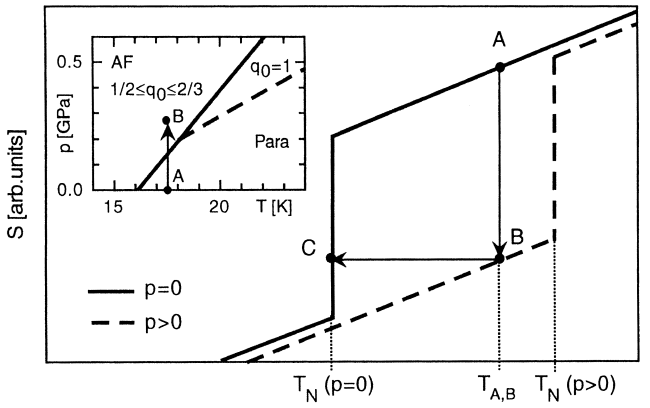

Fig. 2. Schematic plot of the temperature and pressure dependence of the entropy for CeSb. The insert shows the magnetic phase diagram of CeSb.

the discontinuity of the entropy at T_N which was determined by heat capacity measurements to be $\Delta S \approx 2$ J/mol·K [6], comparable to the refrigerant capacity reported for the 'giant' magnetocaloric effect [4].

Let us now assume that the system is in the paramagnetic state at a temperature $T > T_N$, say at the point A in Fig. 2. We now perform the process of isothermal pressurization such that the system transforms into the magnetically ordered state, thereby moving vertically to the point B. For the next step, the sample has to be isolated from its surroundings, so that the process is adiabatic. The sample is depressurized and moves horizontally to the point C. This process is the barocaloric effect which lowers the temperature of the system. The cooling was verified in barocaloric experiments on a CeSb single crystal [14]. The results obtained for $P = 0.26$ GPa are shown in Fig. 3. The temperature evolution of the cooling rate nicely follows the expectations visualized in Fig. 2. Efficient cooling ΔT is achieved in the temperature interval $16 < T < 21$ K. The cooling increases linearly upon raising the initial sample temperature, until a maximum cooling of $\Delta T \approx -1$ K is achieved. So far, a maximum cooling effect of $\Delta T \approx -2$ K has been observed for $P = 0.52$ GPa at an initial sample temperature of 21 K [14].

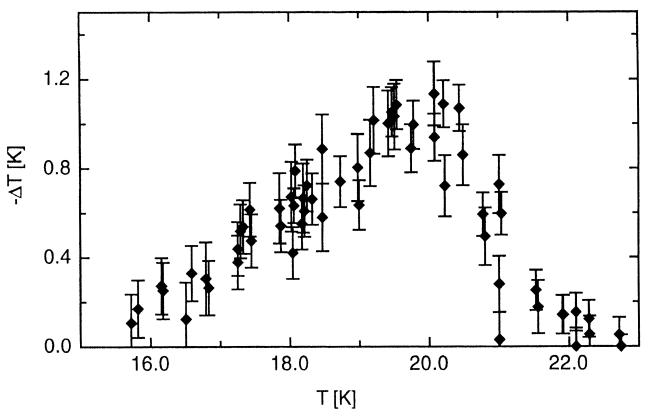

Fig. 3. The barocaloric effect ΔT observed in CeSb upon releasing a uniaxial pressure of 0.26 GPa.

In order to decrease the working temperature from around 20 K down to the technically more interesting range below 4 K, experiments were performed for the diluted $Ce_{1-x}(Y,La)_xSb$ system. By partial substitution of Ce by non-magnetic Y or La the magnetic ordering temperature is shifted downwards, typically by 5 K per 10% Y or La substitution [15]. Indeed, we have verified the lowering of T_N upon dilution by neutron diffraction experiments on a single crystal of $Ce_{0.85}(La_{0.95}Y_{0.05})_{0.15}Sb$ which shows the onset of short-range magnetic correlations below 7.8 K. By the application of uniaxial pressure ($P > 0.1$ GPa) the magnetic fluctuations are found to develop long-range magnetic ordering [14]. The critical temperature is raised at a rate $dT_N/dp \approx 13$ K/GPa which is considerably larger than for undiluted CeSb and therefore highly beneficial for the efficiency of the barocaloric effect. As a consequence cooling by adiabatic pressure removal could be observed down to 2 K [16]. Similar cooling features were found in barocaloric experiments performed for HoAs ($T_N \approx 5$ K) in the same temperature range [17].

3. The pseudogap in high-temperature superconductors

The δ-function in the neutron cross-section for crystal-field transitions (Eq. (4)) only applies for non-interacting rare-earth ions. However, the crystal-field states are subject to interactions with phonons, spin fluctuations, and charge carriers, which limit the lifetime of the excitation, thus the observed crystal-field transitions exhibit line broadening. The interaction with the charge carriers is by far the dominating relaxation mechanism in metallic rare-earth compounds. The corresponding linewidth $\Gamma_n(T)$ increases almost linearly with temperature according to the well-known Korringa law [18]:

$$\Gamma_n(T) = 4\pi(g-1)^2 J(J+1)[N(E_F)\cdot j_{ex}]^2 \cdot T \qquad (6)$$

where g denotes the Landé factor, $N(E_F)$ the density-of-states of the charge carriers at the Fermi energy E_F, and j_{ex} the exchange integral between the charge carriers and the 4f electrons of the rare-earth ions (the inclusion of crystal-field effects slightly modifies the low-temperature limit of Eq. (6) [19]). In superconducting compounds, however, the pairing of the charge carriers creates an energy gap Δ below the superconducting transition temperature T_c, thus crystal-field excitations with energy $\hbar\omega < 2\Delta$ do not have enough energy to span the gap, and consequently there is no interaction with the charge carriers. For an isotropic gap function the intrinsic linewidth in the superconducting state is then given by

$$\Gamma_s(T) = \Gamma_n(T)\exp\left\{-\frac{\Delta}{k_B T}\right\} \quad (7)$$

This means that $\Gamma_s(T \ll T_c) \approx 0$, and line broadening sets in just below T_c where the superconducting gap opens. The exponential temperature dependence of $\Gamma_s(T)$ was nicely demonstrated in the first neutron spectroscopic study on the classical superconductor $La_{1-x}Tb_xAl_2$ [20]. On the other hand, neutron experiments on the high-T_c compound $Ho_{0.1}Y_{0.9}Ba_2Cu_3O_7$ [19] revealed an unusual temperature dependence, i.e. $\Gamma_s(T)$ does not follow the behavior predicted by Eq. (7), but increases already far below T_c. This was ascribed to a high degree of gap anisotropy, since an anisotropic gap function gives rise to certain relaxation channels even at the lowest temperature, particularly along the directions involving nodes. An anisotropic gap function was also inferred from neutron crystal-field studies on the slightly underdoped high-T_c compounds $HoBa_2Cu_4O_8$ and $Er_2Ba_4Cu_7O_{15}$. However, in these measurements, the normal-state behavior is fully recovered only at $T^* \approx 170$ K [21], i.e. far above $T_c \approx 80$ K, which clearly supports the existence of a pseudogap. Neutron spectroscopy was also applied to study the doping dependence of the pseudogap in $HoBa_2Cu_3O_x$ ($6.4 < x < 7.0$) [22].

The existence of a pseudogap in the electronic excitation spectra of underdoped high-T_c superconductors is considered to be among the most important features of cuprates. The pseudogap phenomena mean the suppression of low-frequency spectral weight in the normal state above T_c. The experimental discovery of the pseudogap gave rise to an impressive number of models for the mechanism that causes the Cooper pairs to form [23]. Experiments searching for an isotope effect on the pseudogap temperature T^* are therefore crucial to discriminate between the different pairing scenarios. In the following we report the results of neutron spectroscopic investigations of the isotope effect on the relaxation rate of crystal-field excitations in $HoBa_2Cu_4O_8$ (i.e. exchange of both ^{16}O vs. ^{18}O and ^{63}Cu vs. ^{65}Cu). This compound is ideal for such studies because it is (slightly) underdoped and highly stoichiometric.

Fig. 4 shows neutron spectra observed for $HoBa_2Cu_4^{18}O_8$ at low energy transfers. There are two strong ground-state crystal-field transitions at energies $\hbar\omega_1 = 0.6$ meV and $\hbar\omega_2 = 1.3$ meV, i.e. $\hbar\omega_i \ll 2\Delta$ (≈ 66 meV [21]). With increasing temperature, the crystal-field transitions exhibit line broadening. In addition, excited crystal-field states become increasingly populated giving rise to excited crystal-field transitions. The energy spectra were fitted according to the neutron cross-section (Eq. (4)) with fixed crystal-field parameters B_n^m taken from Ref [21]. The only free parameters were then an overall scale factor for the intensities and a temperature-dependent linewidth $\Gamma(T)$. The results of the fitting procedure are shown by solid lines in Fig. 4. Fig. 5 displays the temperature dependence of the intrinsic linewidth in reduced units. The linewidth is zero at the lowest temperatures, then it

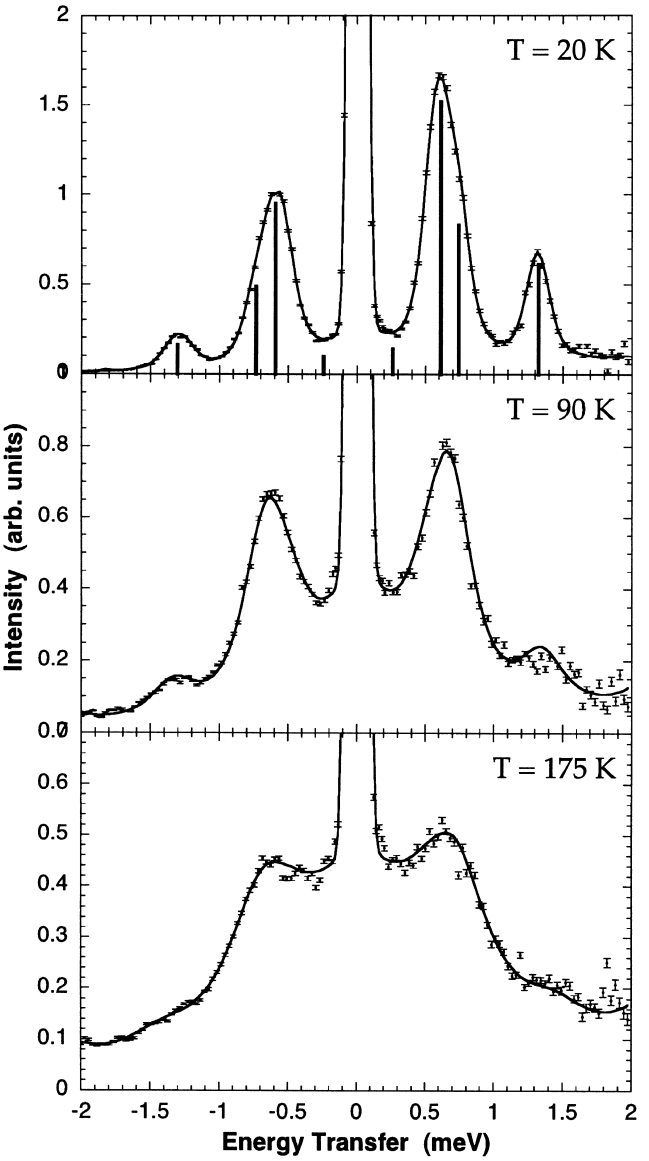

Fig. 4. Energy spectra of neutrons scattered from $HoBa_2Cu_4^{18}O_8$. The vertical bars indicate the positions of the crystal-field transitions. The lines are least-squares fits to the data as described in the text.

increases up to 210 K. A step-like enhancement occurs between 210 and 220 K. Above 220 K, the linewidth follows the Korringa behavior (Eq. (6)) expected for the normal state. We therefore identify the temperature where the step-like enhancement occurs with the temperature where the pseudogap opens, i.e. we set $T^* \approx 220$ K. The linewidth observed for the ^{16}O compound exhibits a similar relaxation behavior (Fig. 5), but the step-like enhancement occurs at much lower temperatures between 160 and 170 K, i.e. $T^* \approx 170$ K [24]. These experiments give evidence therefore for a large oxygen isotope effect $\Delta T^* \approx 50$ K on the pseudogap.

Very recently, neutron spectroscopic experiments were performed on $HoBa_2Cu_4O_8$ to search for a copper isotope effect on the pseudogap [25]. The analysis of the linewidth

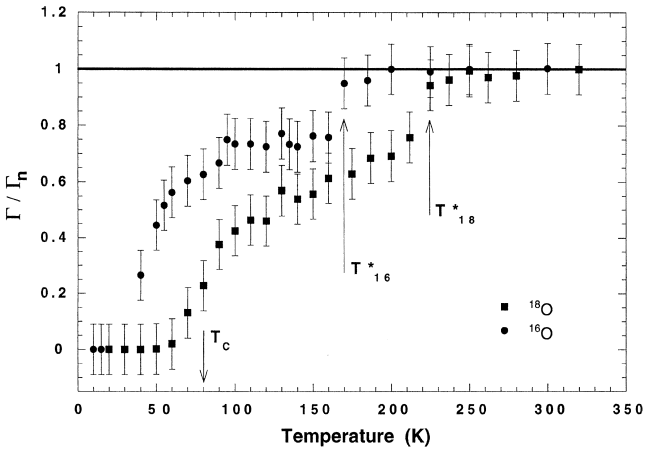

Fig. 5. Temperature variation of the reduced intrinsic linewidth observed for the low-energy crystal-field transitions in both ^{16}O- and ^{18}O-substituted $HoBa_2Cu_4O_8$.

data yields $T^* \approx 160$ K and $T^* \approx 185$ K for the ^{63}Cu and ^{65}Cu compounds, respectively, i.e. $\Delta T^* \approx 25$ K. The large copper and oxygen isotope shifts in T^* suggest that phonons or lattice fluctuations involving both the oxygen and the copper ions are important for the pairing mechanism. Indeed, recent theoretical investigations [26,27] demonstrated that a model involving strong nonlinear electron–phonon effects is able to explain quantitatively the observed isotope shifts in T^*.

3.1. Concluding remarks

In this paper, we have described two exciting developments in the current research on rare-earth compounds for which the crystal-field concept is essential for the understanding of the underlying physical phenomena. This research benefits from the fact that the crystal-field interaction has been well understood for a long time thanks to many pioneering works in this field, starting in the year 1929 with the group-theoretical treatment by Bethe [28] and subsequent developments of suitable operator techniques by Stevens [1] and others. On the experimental side, neutron spectroscopy has played a key role in establishing the crystal-field level splittings in myriads of metallic rare-earth compounds. The latter fact has been and will be essential in the selection of materials exhibiting a 'giant' barocaloric effect as discussed in Section 2. Finally, the observation of large copper and oxygen isotope effects on the pseudogap temperature T^* (Section 3) may be of crucial importance to discriminate between the different models of high-T_c superconductivity, since the pseudogap phenomena are widely regarded as being linked to the pairing mechanism. Here the key role of neutron crystal-field spectroscopy is due to the fact that it is — unlike other techniques — a fast (time scale $\approx 10^{-13}$ s) and local (a few angstroms) method probing the bulk properties.

Acknowledgements

Financial support by the Swiss National Science Foundation is gratefully acknowledged. We are indebted to K.A. Müller for stimulating discussions as well as to K. Conder, S. Janssen, J. Karpinski, P. Lacorre, K. Mattenberger, J. Mesot, H. Mutka and V. Trounov for co-operation in part of the experimental work.

References

[1] K.W.H. Stevens, Proc. Phys. Soc. A 65 (1952) 209.
[2] G.T. Trammell, Phys. Rev. 92 (1953) 1387.
[3] O. Moze, in: K.H.J. Buschow (Ed.), Handbook of Magnetic Materials, Vol. 11, Elsevier, Amsterdam, 1998, p. 493.
[4] V.K. Pecharsky, K.A. Gschneidner Jr, Phys. Rev. Lett. 78 (1997) 4494.
[5] A. Furrer, K.A. Müller, J. Mesot, Swiss Patent Application No. 2730/97 (November 1997) and International Patent Application No. PCT/IB98/01879 (November 1998).
[6] T. Strässle, Diploma Thesis. ETH, Zurich, 1999.
[7] S. Rosenkranz, M. Medarde, F. Fauth, J. Mesot, M. Zolliker, A. Furrer, U. Staub, Ph. Lacorre, R. Osborn, R.S. Eccleston, V. Trounov, Phys. Rev. B 60 (1999) 14857.
[8] K.A. Müller, F. Fauth, S. Fischer, M. Koch, A. Furrer, P. Lacorre, Appl. Phys. Lett. 73 (1998) 1056.
[9] J. Rossat-Mignod, P. Burlet, J. Villain, H. Bartholin, W. Tcheng-Si, D. Florence, O. Vogt, Phys. Rev. B 16 (1977) 440.
[10] P. Fischer, B. Lebech, G. Meier, B.D. Rainford, O. Vogt, J. Phys. C 11 (1978) 345.
[11] F. Lévy, Phys. Konden. Mater. 10 (1969) 85.
[12] B. Hälg, A. Furrer, O. Vogt, Phys. Rev. Lett. 57 (1986) 2745.
[13] H. Heer, A. Furrer, W. Hälg, O. Vogt, J. Phys. C 12 (1979) 5207.
[14] T. Strässle, A. Furrer, K.A. Müller, Physica B 276–278 (2000) 944.
[15] B. Hälg, A. Furrer, O. Vogt, Phys. Rev. Lett. 54 (1985) 1388.
[16] T. Strässle, A. Furrer, High Pressure Res. 17 (2000) 325.
[17] T. Strässle, K. Mattenberger, A. Furrer, J. Alloys Comp. 323–324 (2001) 392.
[18] J. Korringa, Physica 16 (1950) 601.
[19] A.T. Boothroyd, A. Mukherjee, A.P. Murani, Phys. Rev. Lett. 77 (1996) 1600.
[20] R. Feile, M. Loewenhaupt, J.K. Kjems, H.E. Hoenig, Phys. Rev. Lett. 47 (1981) 610.
[21] J. Mesot, G. Böttger, H. Mutka, A. Furrer, Europhys. Lett. 44 (1998) 498.
[22] D. Rubio, J. Mesot, K. Conder, S. Janssen, H. Mutka, A. Furrer, J. Supercond. 13 (2000) 727.
[23] For a recent review of the pseudogap see: B. Batlogg, C. Varma, Phys. World, February 2000, p. 33.
[24] D. Rubio Temprano, J. Mesot, S. Janssen, K. Conder, A. Furrer, H. Mutka, K.A. Müller, Phys. Rev. Lett. 84 (2000) 1990.
[25] D. Rubio Temprano, J. Mesot, S. Janssen, K. Conder, A. Furrer, A. Sokolov, V. Trounov, S. Kazakov, J. Karpinski, K.A. Müller, J. Alloys Comp. 323–324 (2001) 554.
[26] A. Bussmann-Holder, A. Simon, H. Büttner, A.R. Bishop, Phil. Mag. B 80 (2000) 1955.
[27] A. Bussmann-Holder, J. Supercond. 13 (2000) 773.
[28] H. Bethe, Ann. Phys. 3 (1929) 133.